Materials Science-Poland, Vol. 26, No. 3, 2008

Structural, optical, electrical and magnetic properties of sol-gel derived $Zn_{1-x-y}Co_xAl_yO$ films

M. SHARMA, R. M. MEHRA*

Department of Electronic Science, University of Delhi, South Campus, New Delhi 110021, India

A detailed study has been presented of optical, electrical, structural and magnetic properties of $Zn_{1-x}Co_xO$ ($0 < x \leq 0.25$) films co-doped with 1 at. % of Al. The polycrystalline films have been synthesized on Corning glass 7059 substrates by the sol-gel technique using spin coating. Highly preferential *c*-axis oriented films have been obtained at the annealing temperature of 600 °C. The lattice constant *d* of *c*-axis wurtzite $Zn_{1-x-y}Co_xAl_yO$ obeys Vegard's law for ($0 < x \leq 0.25$). The inclusion of Al in ZnO is highly beneficial for the magnetism in ZnO because it enhances the free electron density. Optical spectra measurements reveal that band gap energy exhibits a blue shift upon increasing Co concentration. A positive magnetoresistance for Co doped ZnO and negative magnetoresistance for ZnO without cobalt at 77 K has been observed. The ferromagnetic behaviour has been confirmed by measurements using superconducting quantum interference device. The coercive field and the remanence increase with increase in Co content.

Key words: *sol-gel; ZnO:Co; dilute magnetic semiconductor; hysteresis*

1. Introduction

An exciting possibility to utilize both the charge and spin character of an electron to develop spintronic devices such as spin field effect transistors (FETs) and spin light emitting transistors (LEDs) [1, 2] has led to extensive search for materials in which semiconducting properties can be integrated with magnetic properties. These materials are categorized as dilute magnetic semiconductors (DMSs) which are fabricated by introducing small fractions of transition metals (TMs) into host (non magnetic) semiconductors, e.g., III–V [3] and II–VI compounds [4]. The essential requirement for achieving practical spintronic devices is efficient electrical injection of spin-polarized carriers [5]. The material should be capable of transporting the carriers with high transmission efficiency in the host semiconductor.

*Corresponding author, e-mail: rammehra2003@yahoo.com

These key aspects of spin injection, spin dependent transport manipulation and detection form the basis for current research and future technology [3]. Low power consumption of these devices has the advantage of resulting in high packing densities for memory elements [6]. Thus from industrial application point of view it is important for DMS to be an efficient conductor and ferromagnetic at room temperature. In 1998, Ohno [7] reported existence of ferromagnetic behaviour in Mn doped GaAs with the Curie temperature T_c of 100 K. Unfortunately, the highest T_c reported to date was 172 K [8]. This caused researchers to search for other material systems.

Recent studies have identified wide band gap semiconductors including GaN and ZnO systems as promising materials for spintronics applications [9]. From the point of view of industrial application (opto- and magnetoelectronics) ZnO with exciton binding energy of 63 meV and 3.3 eV bandgap has many attractive aspects such as low cost, abundance, and, in addition, it is environmentally friendly [10]. Moreover, it is transparent to visible light and has a higher TM solubility. Dietl et al. [11] made theoretical predictions for room temperature ferromagnetism (RTFM) in heavily doped p-type ZnO alloy. Since p-type ZnO is difficult to fabricate [10], much work has been pursued on n-type ZnO with various TM dopants. Co was chosen as its ionic radius matches to that of Zn^{2+} ion resulting in high solubility [12]. Al is a good co-dopant as it is an adequate electron donor and has no d electrons to interfere with magnetic ordering. Early experimental work has provided mixed and even contradicting results. In one of the studies of doping various TMs into ZnO by Ueda et al. [13] highly conducting n-type Co doped ZnO displayed room temperature ferromagnetism. Research studies [14–16] confirmed these findings. Other studies found that ferromagnetism is extrinsic in nature and arises from nanoclusters and secondary magnetic phases [17–19].

We need to study $Zn_{1-x-y}Co_xAl_yO$ system in detail to understand its structural, electrical and optical properties as they play an important role in promoting ferromagnetism (FM) and in determining the origin of ferromagnetism. We have grown thin films of $Zn_{1-x-y}Co_xAl_yO$ on Corning glass substrate by sol-gel process with high pH sol. Sol -gel technique has advantages in fabricating DMS sample because the mole fractions can be controlled accurately and samples with various compositions can be easily obtained.

2. Experimental

The precursor sols were prepared from zinc acetate dihydrate $Zn(CH_3COO)_2{\cdot}2H_2O$ (Merck Extra Pure Chemical Ind. Ltd, India, purity 99.95%)), methanol (AR, Merck Chemicals, India) and monoethanolamine [MEA] (Merck, India). Cobalt acetate hexahydrate $Co(CH_3COO)_2.6H_2O$ (AR, Merck Chemical Ind. Ltd, India, purity 99.9%) was introduced as a dopant in at. % varying from 5 to 25. Aluminium chloride $AlCl_3$ (Merck, India) was also introduced into the sol in 1 at. %. pH of the solution was 9 with MEA/ZnAc weight ratio as 1. The obtained mixture was stirred using magnetic stirrer for about 60 min to obtain clear homogeneous solution. Microscopic Corning glass (7059) slide substrates were cleaned ultrasonically, first in acetone and then sub-

sequently in methanol for 10 min each. They were further cleaned with deionised water for 20 min and finally dried in nitrogen atmosphere. The clear solutions were used after 48 h for spin coating. The spinning speed and time were optimized to 3000 rpm and 20 s, respectively, to ensure that each spun layer is thin enough to ensure simultaneous evaporation of all solvent, thus preventing cracking of the films. The wet films were kept to hydrolyze in air at room temperature for 5 min, and then were dried at 300 °C for next 10 min. The drying process removes the residual organic solvents and organic groups in the deposited gel film and converts the organic precursor film into a dense inorganic film. An approximate thickness of 15 nm was obtained for each spin. The above process of coating and drying was repeated several times to increase the film thickness and to get the desired thickness. Finally the deposited films were annealed in air in the temperature range of 400–600 °C for 1 h. A slow cooling rate was maintained to avoid the possibility of stress in the films as expected in rapid cooling.

Crystallite phase and orientation were evaluated by the X-ray diffraction method (XRD, Philips PW 1830 Geiger counter diffractometer, PW 3710) using a monochromatized X-ray beam with nickel-filtered CuK_α radiation (λ = 1.54 Å) operating at 40 kV and 20 mA. A continuous scan mode was used to collect 2θ data from 20° to 50°, with a 0.02 sample pitch and 3 deg/min scan rate. The compositions of Co and Al doped ZnO films were determined by the elemental dispersion analysis using X-ray (EDAX) measurements (SEM, LEO 435VP, UK). Average surface roughness R_a and crystallite size were measured by the atomic force microscopy (Burleigh-SPI 3700). Images were recorded via a multimode scanning probe microscope (Digital Instruments). We have used a contact mode with the constant force method (the force between the sample surface and the tip was kept constant by a feedback system while the surface beneath the tip was scanned). The thicknesses of the films were determined by SANTEC ellipsometry and it was found to lie in the range of 200 nm. Optical characterization was performed in the wavelength range of 250–1000 nm using a Solidspec UV-3700 spectrophotometer. The electrical conductivity σ and magnetoresistance were measured by the van der Pauw technique. Contacts for transport measurement were made by pressed indium. The sign of the Hall coefficient confirmed the n-type conduction of the films. The magnetic properties of the sample were characterized using commercial superconducting quantum interference device SQUID (Quantum Design, USA) magnetometer.

3. Results and discussion

3.1. Chemical analysis on $Zn_{0.94}Co_{0.05}Al_{0.01}O$ thin film (EDAX)

Composition analysis of $Zn_{0.94}Co_{0.05}Al_{0.01}O$ film is shown in Fig. 1. The film annealed at 600 °C for 1 h in air atmosphere showed the presence of zinc, cobalt and aluminium. No other impurity was found within the EDAX detection limit.

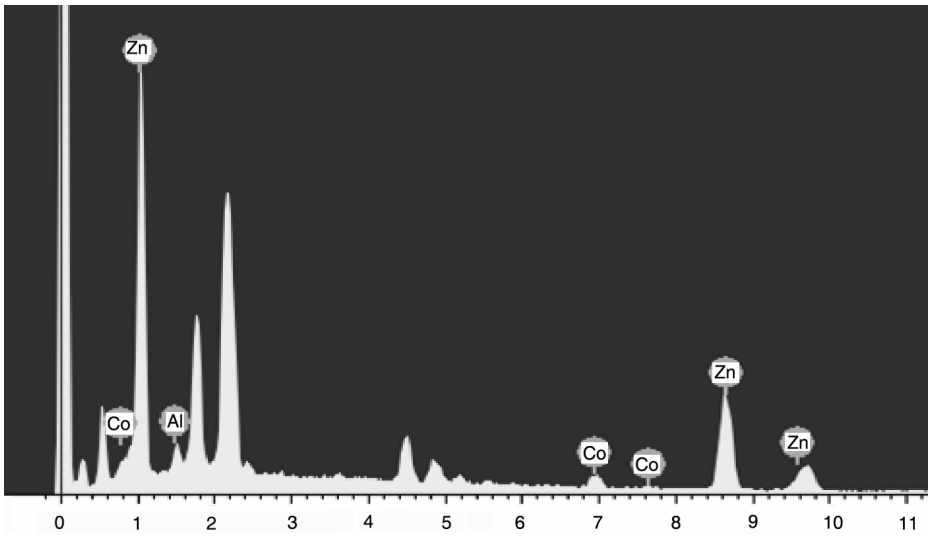

Fig. 1. Energy dispersive X-ray analysis spectrum of $Zn_{0.94}Co_{0.05}Al_{0.01}O$ film annealed at 600 °C

3.2. Structural analysis

Figure 2 shows the XRD patterns of $Zn_{0.95}Co_{0.05}Al_{0.01}O$ in function of annealing temperature T_a. It shows an evidence of polycrystalline structure with (100), (002) and (101) peaks. Upon increase of T_a from 400 °C to 600 °C, the intensity of (002) reflection peak increases. The film grown at 600 °C exhibits a highly *c*-axis preferential growth.

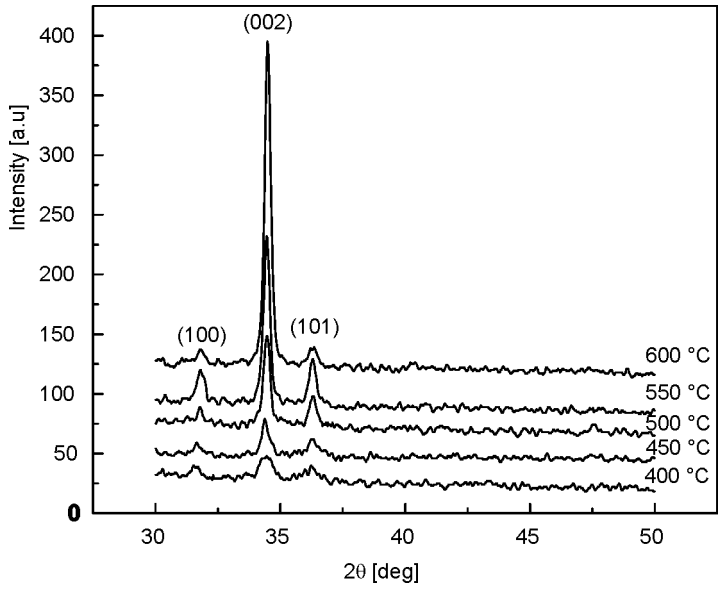

Fig. 2. X-ray diffraction patterns of $Zn_{0.94}Co_{0.05}Al_{0.01}O$ films grown at various temperatures

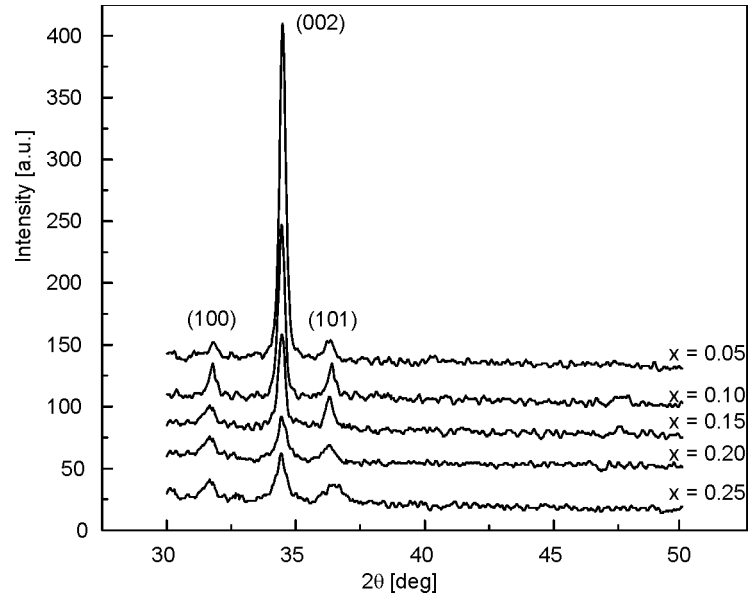

Fig. 3. X-ray diffraction patterns of $Zn_{1-x-y}Co_xAl_yO$ (x = 0.05–0.25, y = 0.01) films annealed at 600 °C

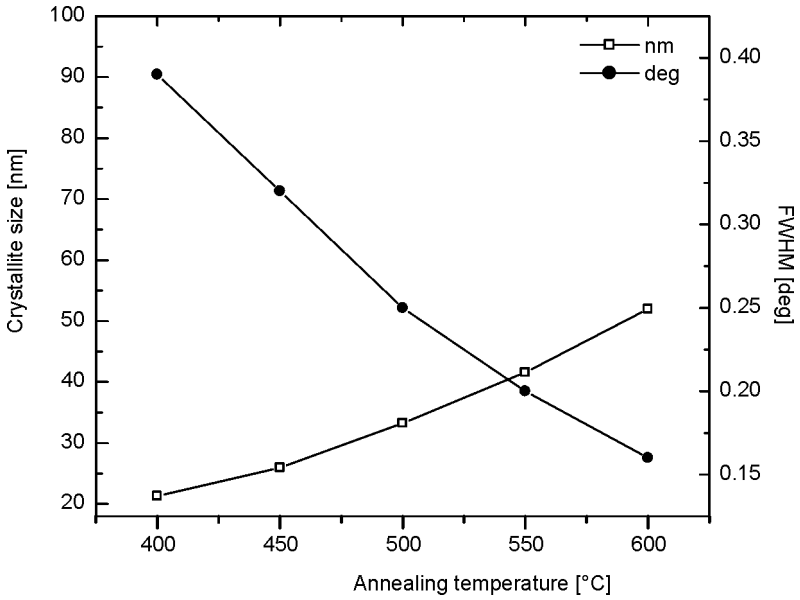

Fig. 4. Dependence of annealing temperature on crystallite size and full width half maximum (FWHM)

Figure 3 shows the X-ray diffraction patterns of the $Zn_{1-x}Co_xO$:Al films annealed at the optimized temperature (600 °C) with various Co concentrations x (0.05–0.25).

The films exhibit a dominant peak at $2\theta = 34.43°$ corresponding to the (002) plane of ZnO, and other peaks corresponding to (100) and (101) indicating the polycrystalline nature of the films. It is seen from the figure that the relative intensity of the (002) peak decreases with increasing Co dopant concentration. No peaks corresponding to either (111) peak Co (44.217) or 400 peak Co_2O_4 (44.74) or (400) peak Co_3O_4 (44.81) appear in the diffraction pattern of the samples, suggesting that Co is incorporated well at the Zn lattice site in the hexagonal wurtzite structure of ZnO. (102) peak for ZnO (47.539) is observed in some samples. We do not exclude the possibility of formation of clusters small enough not to be detected by XRD. Crystallite size was calculated from the Scherrer's equation [20] based on the (002) plane. It is observed in Fig. 4 that the full width half maximum (FWHM) decreases and crystallite size increases with the increase in annealing temperature. The values of crystallite sizes at various T_a are listed in Table 1.

Table 1. Crystallite sizes (t) determined from XRD data and AFM images for $Zn_{0.94}Co_{0.05}Al_{0.01}O$ films at various annealing temperatures (T_a)

T_a [°C]	t [nm]	
	XRD	AFM
450	25.9	20
500	33.2	35
550	41.5	49
600	51.9	59

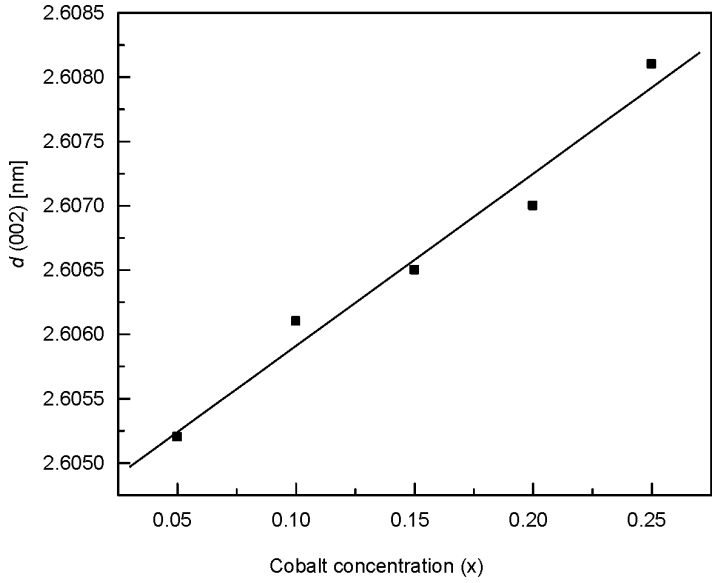

Fig. 5. Dependence of c-axis lattice constants (d(002) values) on Co content in $Zn_{1-x}Co_xO$:Al films

The interplanar spacing *d* in the direction of *c* axis (002) in function of Co content is shown in Fig. 5. It is seen from the figure that the *d* values increase upon increase of the Co content up to 25% in accordance with Vegard's law. Thus up to 25% Co lies within solubility limit of substitution. Cobalt exists in the divalent state, and high solubility of Co is attributed to the ionic radius of Co^{2+} (72 pm) being similar to that of Zn^{2+} (74 pm) in the tetrahedral coordinated structure. Ueda et al. [13] showed a similar dependence of *d* on Co concentration for PLD grown ZnO films co-doped with Co and 1% of Al.

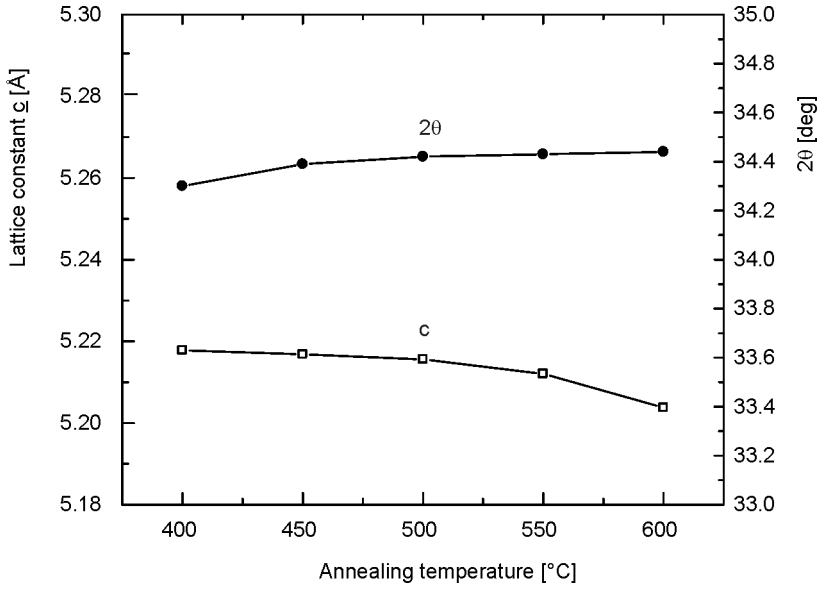

Fig. 6. Effect of annealing temperature on the lattice constant *c* and diffraction angle 2θ of (002) peak of $Zn_{0.94}Co_{0.05}Al_{0.01}O$ films

Figure 6 shows the variation of the diffraction angle 2θ of (002) peak and lattice constant *c* with the annealing temperature. A shift in the (002) peak 2θ position to a slightly higher value is observed with the increase in the annealing temperature and it approaches near to the powder value of 34.44° at 600 °C. It is important to note that the value of the *c* lattice parameter for the as deposited $Zn_{0.95}Co_{0.05}O$:Al films is large in comparison to unstressed bulk value of 5.207 Å [12]. This is consistent with other works reporting increase of the *c* axis lattice constant with increase in Co concentration in doped ZnO films [13]. A large value of the lattice constant for the as grown and annealed compared to the unstressed powder value shows that the unit cell is elongated along the *c* axis, and compressive forces act in the plane of the film. This indicates a reduction in the tensile stress with annealing, which may be due to the large coefficient of linear expansion of films in comparison with the glass substrate with increase in the annealing temperature. The higher value of *c* at 400 °C shows that the unit cell is elongated along the *c* axis, and compressive forces act in the plane of the films.

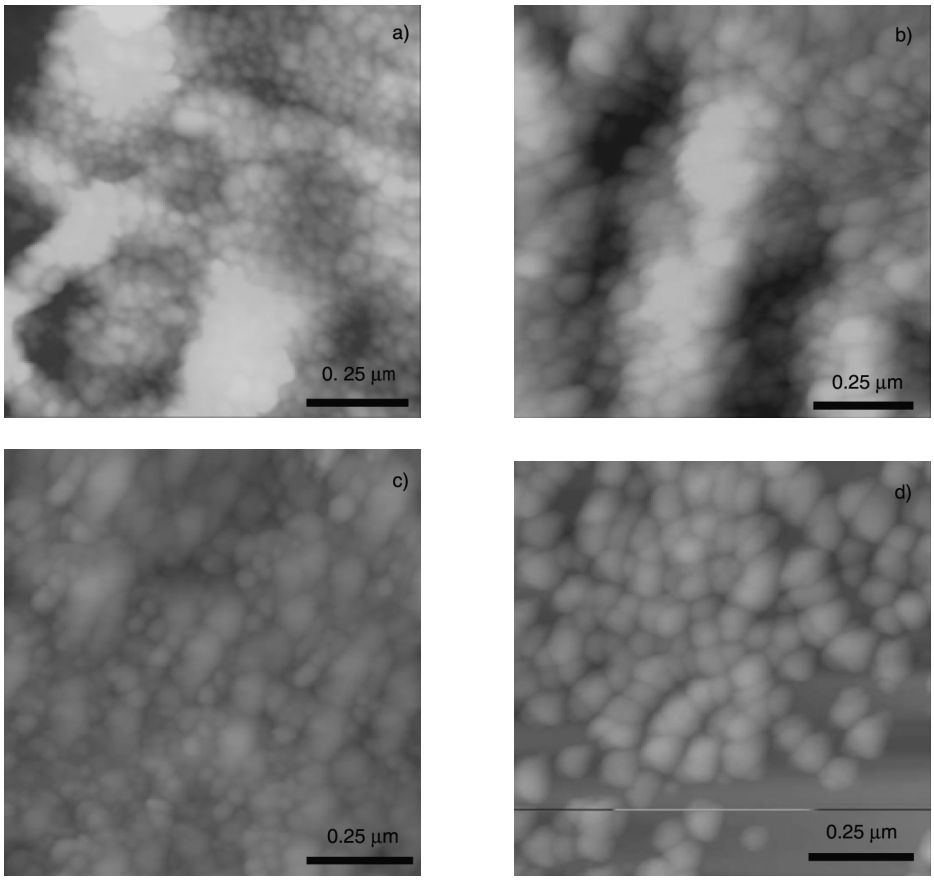

Fig. 7. AFM images of $Zn_{0.94}Co_{0.05}Al_{0.01}O$ films annealed at: a) 450 °C, b) 500 °C, c) 550 °C, d) 600 °C

Figure 7 shows the AFM graphs of the surfaces of deposited films for Co dopant concentration $x = 0.05$, annealed at various temperatures. The formation of a fine surface having uniformly distributed grains and gradual increase in grain size is clearly observed in films annealed at a higher temperature of 600 °C. The minimum average roughness 5 nm, which was obtained for the film grown at 600 °C, originates from the craters between the grain boundaries and the contribution of the substrate roughness to the first layer of the film. These values of grain size are also listed in Table 1. It is seen from the table that the value of grain size correspond well with the values obtained from XRD measurements by the Scherrer–Warren formula

$$t = \frac{0.94\lambda}{\beta \cos\theta}$$

where t is the crystallite size in nm, λ is wavelength in nm, β is the FWHM of the (002) peak and θ is the angle of the (002) peak.

3.3. Transmittance

Figure 8 shows optical transmission spectra of $Zn_{1-x-y}Co_xAl_yO$ films annealed at 600 °C and recorded in the wavelength region of 300–1000 nm for various Co contents

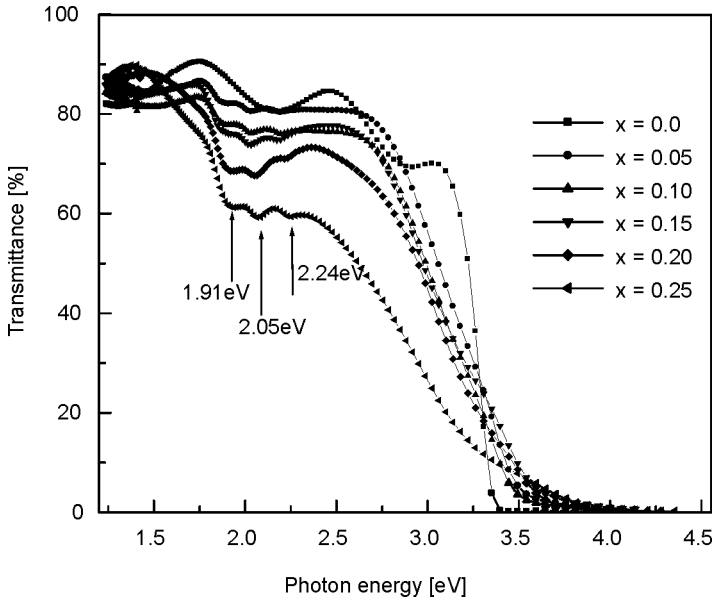

Fig. 8. Optical transmission spectra of sol-gel deposited $Zn_{1-x}Co_xO$:Al films recorded at room temperature for various Co contents x and 1 at. % of Al

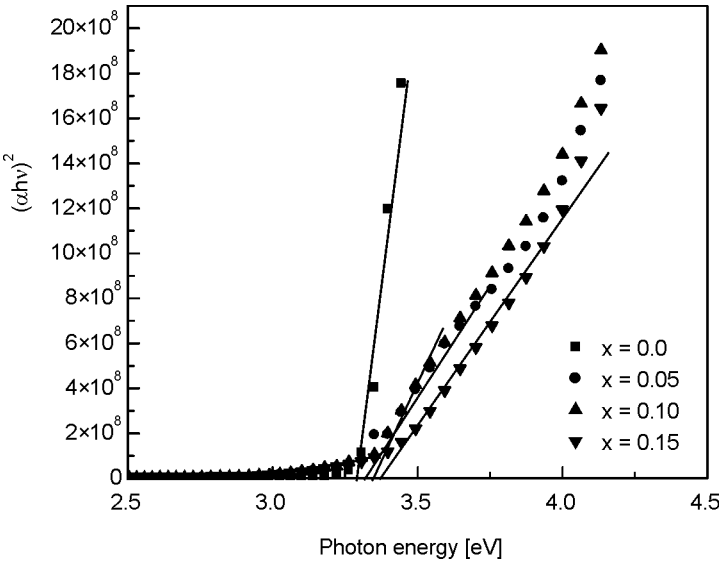

Fig. 9. Optical absorption spectra of $Zn_{1-x}Co_xO$:Al films

x = (0–0.25). The transmission is found to be maximum for the sample without Co and decreases with the increase in Co concentration. The fundamental edge for thin films is located at 3.26 eV. The decrease in optical transmission is associated with the loss of light due to (i) oxygen vacancies and (ii) scattering at grain boundaries. The increase in scattering centres due to increased number of grain boundaries with an increase in Co dopant content may be responsible for the loss of transmission. A decrease in grain size and thereby increase in grain boundaries in $Zn_{1-x-y}Co_xAl_yO$ film upon increasing Co concentration has been observed. We attribute absorption bands at about 1.9, 2.05, 2.24 eV to the d-d transitions of tetrahedral coordinated Co^{2+} which are assigned to $^4A_2(F) \rightarrow {}^2E(G)$, $^4A_2(F) \rightarrow {}^4T_1(P)$, $^4A_2(F) \rightarrow {}^2A_1(G)$, transitions in the high spin state of $Co^{2+}(3d^7)$, respectively [17]. The figure shows clearly that intensities of the absorption bands increase with Co content, indicating consistent incorporation of Co^{2+} ions into ZnO lattice in the valence state of 2+ by the sol-gel process.

The band gap energy E_g was determined by using formula the $(\alpha h\nu)^2 = B(E - E_g)$ and plotting the curves $(\alpha h\nu)^2$ vs. E, where α is the absorption coefficient, E is the photon energy and B is a constant. These curves are shown in Fig. 9.

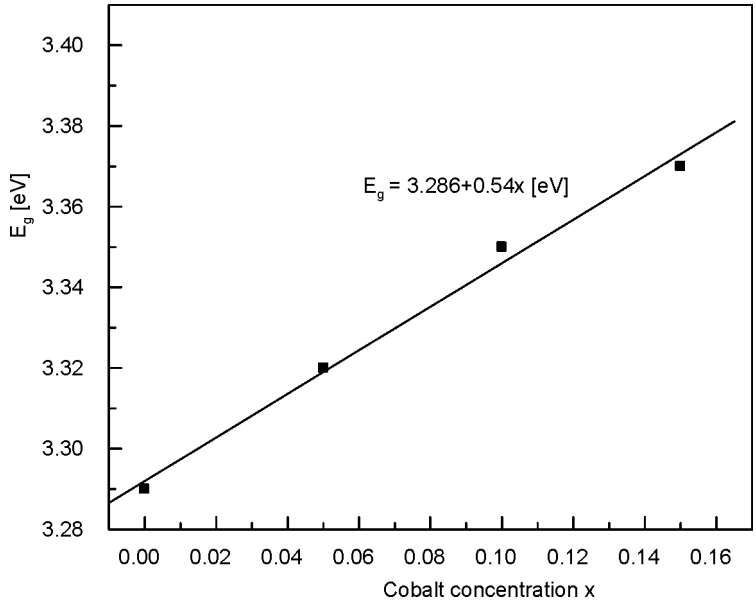

Fig. 10. Dependence of band gap (E_g) of $Zn_{1-x}Co_xO$:Al films on the Co content

Figure 10 shows dependence of E_g on the Co content. The variation of E_g with Co content was found to follow the relationship E_g = (3.286 + 0.54x) eV. It means that the extrapolated value 3.286 eV of the band gap for x = 0 corresponds to the undoped ZnO films. A characteristic difference in the absorption edge has been observed with Co incorporation in ZnO. The sharp absorption edge observed for pure ZnO sample at 3.18 eV was found to start shifting vigorously with an increase in Co concentration.

This blue shift in the optical band gap is also observed in ZnMnO [21], ZnMgO [22]. Kim et al. [17] also showed similar blue shift in PLD deposited $Zn_{1-x}Co_xO$ films. He showed variation of E_g with x up to 30% of Co content.

3.4. Electrical properties

The influence of the annealing temperature from 400 °C to 600 °C on the resistivity ρ, carrier concentration n and Hall mobility μ_H of $Zn_{1-x-y}Co_xAl_yO$ films containing 5 at. % of Co with 0 and 1 at. % of Al is shown in Figs 11 and 12, respectively. It is seen from the figures that the carrier concentration has increased as a result of Al doping. This increase is attributed to the substitutional doping of Al^{3+} at Zn^{2+} sites creating one extra free electron in the conduction band [23]. The major conduction was confirmed to be n-type by the Hall measurements and films exhibited semiconducting behaviour. The resistivity is found to decrease with increasing T_a. The decrease in resistivity with higher temperature is due to an improvement in crystallinity.

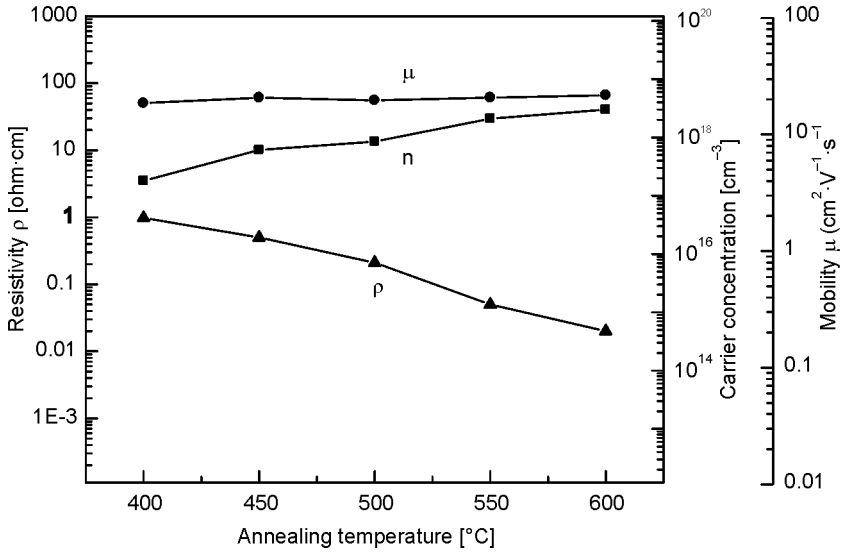

Fig. 11. Resistivity, electron concentration, and Hall mobility in function of annealing temperature for $Zn_{1-x-y}Co_xAl_yO$ ($x = 0.05$, $y = 0$)

The mobility is found to increase upon increasing T_a, which is also due to improvement in the crystalline structure. Figure 12 shows that the value of mobility ranges from 17 to 43.5 cm^2/(V·s) [13]. The carrier concentration is found to increase with increase in T_a. The maximum carrier concentration obtained was 10^{21} cm^{-3} at 600 °C for $Zn_{0.94}Co_{0.05}Al_{0.01}O$. The increase in grain size means a decrease in grain boundaries (lesser scattering area) and pores in the annealed films as compared to the as deposited films. Thus the number of electron trap states reduces and hence the car-

rier concentration increases. Xu et al. [12] declared carrier concentration to vary from 10^{20} to 10^{21} cm^{-3}) for ZnO films co-doped with 5% Co and 1% Al by PLD.

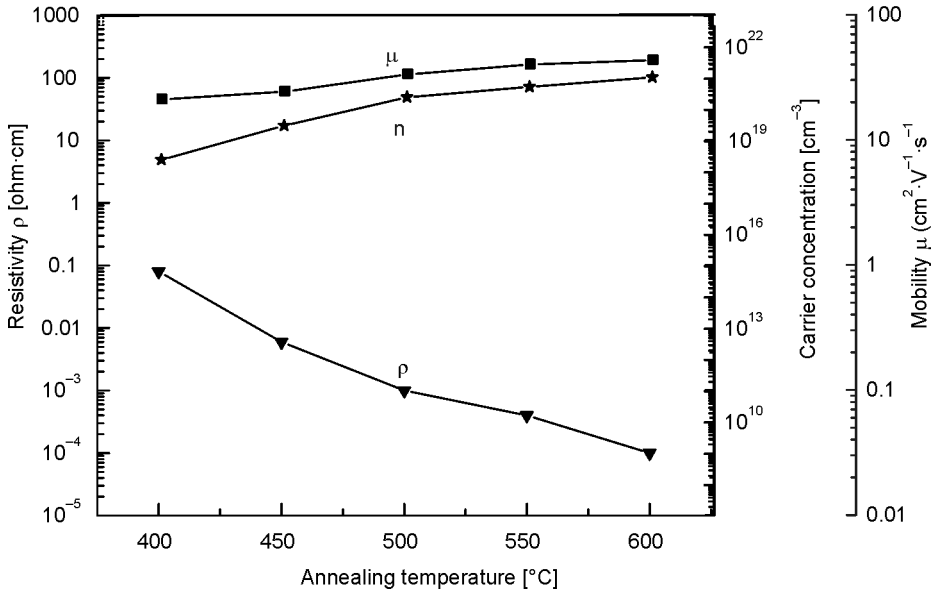

Fig. 12. Resistivity, electron concentration, and Hall mobility in function of annealing temperature for $Zn_{1-x-y}Co_xAl_yO$ ($x = 0.05$, $y = 0.01$)

3.5. Magnetic properties

Figure 13 shows magnetoresistance (MR) at 77 K with magnetic field applied perpendicular to the film plane. MR helps to reveal the nature of fundamental exchange coupling in the DMS. It can be explained in terms of three different competitive mechanisms such as sp-d exchange [24], weak localization [25], spin disorder scattering [26]. Negative MR is due to scattering of spin polarized charge carriers at isolated magnetic impurities. Positive MR can be well understood by the dominance of sp-d exchange interaction over the weak localization effect and spin disorder scattering with increase in Co content.

Films without Co give negative MR as the applied field will align the spins and thus reduce the scattering. Positive MR is seen in Co doped ZnO films. It was found that positive MR increases with increase in Co content.

The magnetic properties were measured with a SQUID magnetometer at room temperature for $Zn_{1-x}Co_xAl_{1-x-y}O$ ($x = 0$, 0.05, 0.10, 0.15) films. The magnetic field is applied parallel to the film plane. Diamagnetic and/or paramagnetic signals of the glass substrate were detected. Figures 14 and 15 show hysteresis loops for various concentrations of Co. The ferromagnetism is clearly shown by the coercivity and remanence. The remanence of the films for higher concentrations is higher than for

lower concentrations of Co. The coercive field for $x = 0.15$ was 10 mT and the estimated saturation magnetization was 8×10^{-9}Am^2 from the field dependence of magneti-

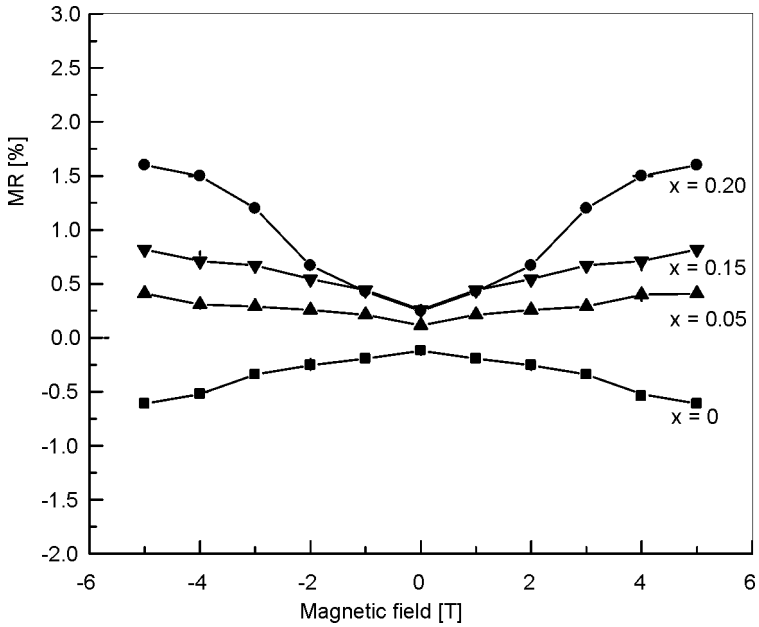

Fig. 13. Magnetoresistance curves for various concentrations of Co at 77 K

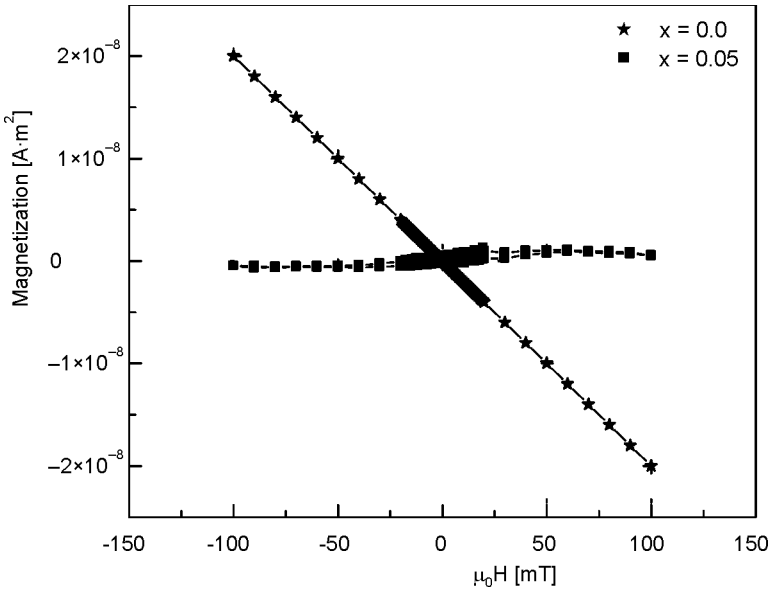

Fig. 14. Magnetization curves measured in plane for $Zn_{1-x}Co_xO$:Al films ($x = 0.0$ and 0.05)

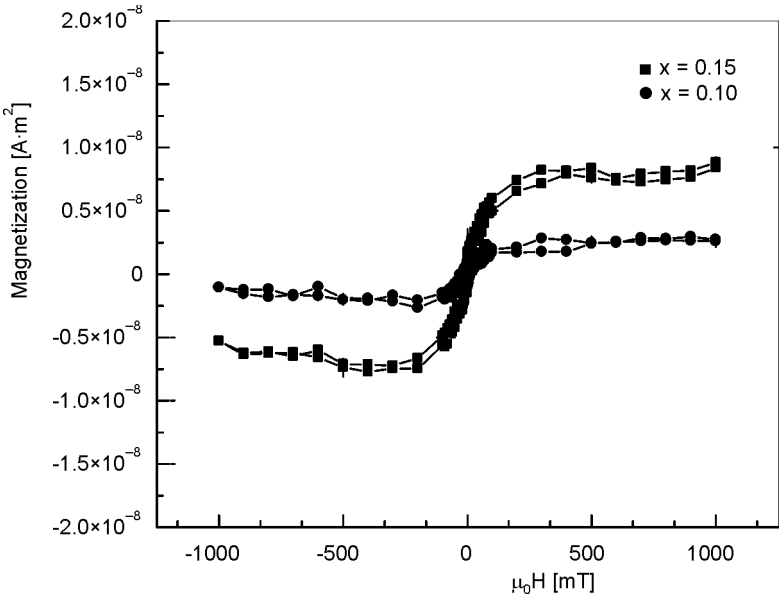

Fig. 15. Magnetization curves measured in plane for $Zn_{1-x}Co_xO$:Al films (x = 0.1 and 0.15)

zation (*M–H*) curve. The saturation field was around 284 mT. In absence of Co dopant, ZnO film exhibits diamagnetic behaviour and Co doped films exhibits hysteresis loops.

4. Conclusion

$Zn_{1-x}Co_xO$ ($0 < x \leq 0.25$) films with 1 at. % of Al doping on Corning glass have been prepared by the sol-gel process. XRD and UV-VIS-NIR spectroscopy results confirm the substitutional doping of Co in the ZnO wurtzite lattice. High conductivity and good transparency were obtained for $Zn_{0.94}Co_{0.05}Al_{0.01}O$ film annealed at 600 °C. The observed positive MR is the representative of DMS nature of the Co doped films. SQUID measurements have further confirmed the ferromagnetic nature of these films. The coercivity and remanence of the films are found to increase with Co concentration.

Acknowledgements

The authors are grateful to Dr. Stephen Weyeneth of the Physics Institute, University of Zürich, Switzerland for the SQUID measurements and discussion. The financial support from the DST, New Delhi for the Solidspec 3700 UV-VIS-NIR spectrophotometer is also gratefully acknowledged.

References

[1] WOLF S.A., AWSCHALOM D.D., BUHRMAN R.A., DAUGHTON J.M., VON MOLNAR S., ROUKES M.L., CHTCHELKANOVA A.Y., TREGER D.M., Science, 294 (2001), 1488.
[2] PRINZ G.A., Science, 282 (1998), 1660.
[3] PEARTON S.J., ABERNATHY C.R., OVERBERG M.E., THALER G.T., NORTON D.P., THEODOROPOULOU N., HEBARD A.F., PARK Y.D., REN F., KIM J., BOATNER L.A., J. Appl. Phys., 93 (2003), 8979.
[4] PRELLIER W., FOUCHET A., MERCEY B., J. Phys. Condes.Matter, 15 (2003), R1583.
[5] *Spin Electronics*, M. Ziese, M.J. Thornton (Eds.), Springer, Berlin, 2001.
[6] BUHRMAN R., WTEC Spin Electronics Workshop, Washington, DC, 2 Nov. 2001 (Viewgraphs from the presentation are available at http://www.wtec.org/spin/views/buhrman/index.htm).
[7] OHNO H., Science, 281 (1998), 951.
[8] NAJMUL A.M., SUGAHARA S., TANAKA M., Phys. Rev., B67 (2003), 241308.
[9] YANG S.G., PAKHOMOV A.B.,.HUNG S.T, WONG C.Y., IEEE Trans. Magn., 37 (2002), 2877.
[10] SATO K., KATYAMA-YOSHIDA H., Jpn. J. Appl. Phys., 40 (2001), L334.
[11] DIETL T., OHNO H., MATSUKURA F, CUBERT J, FERRAND D., Science, 287 (2000), 1019.
[12] XU X.H., BLYTHE H.J., ZIESE M., BEHAN A.J., NEAL J.R., MOKHTARI A., IBRAHIM R.M., FOX A.M., GEHRING G. A., New J. Phys., 8 (2006), 135.
[13] UEDA K., TABATA H., KAWAI T., Appl. Phys. Lett., 79 (2001), 988.
[14] HYEON-JUN LEE, SE-YOUNG JEONG, CHAE RYONG CHO, CHUL HONG PARK, Appl. Phys. Lett., 81 (2002), 4020.
[15] CHO W.K., CHOO Y.M, KIM H., KIM D., IHM Y., Appl. Phys. Lett., 80 (2002), 3358.
[16] RAMACHANDRAN S., TIWARI A., NARAYAN J., Appl. Phys. Lett., 84 (2004), 5255.
[17] KIM J.H., KIM H., KIM D., IHM Y. E. AND CHO W.K., J. Appl. Phys., 92 (2002), 6066.
[18] PARK J.H., KIM M.G., JANG H.M., RYU S., KIM Y.M., Appl. Phys. Lett., 84 (2004), 1338.
[19] BELGHAZI Y., SCHMERBER G., COLIS S., REHSPRINGER J.L., DINIA A., BERRADA A., Appl. Phys. Lett., 89 (2006), 122504.
[20] CULLITY B.D., *Elements of X-Ray Diffraction*, Addison-Wesley, Reading, MA, 1978.
[21] FUKUMURA T., JIN Z., OHTOMO A., KOINUMA H., KAWASAKI M., Appl. Phys. Lett., 75 (1999), 3366.
[22] OHTOMO A., KAWASAKI M., KOIDA T., MARUBUCHI K., SEGAWO Y., Appl. Phys. Lett., 72 (1998), 2466.
[23] SAGAR P., KUMAR M., MEHRA R.M., Mater. Sci.-Poland, 23 (2005), 685.
[24] SAWICKI M., DIETL T., KOSSUT J., IGALSON J., WOJTOWICZ T., PLESIEWICZ W., Phys. Rev. Lett., 56 (1986), 508.
[25] PIKUS F.G., PIKUS G.E., Solid State Commun., 100 (1996), 95.
[26] TOYOZAWA Y., J. Phys. Soc. Japan, 17 (1962), 986.

Received 25 September 2007
Revised 19 November 2007